Available online at www.sciencedirect.com
ScienceDirect
Polymer 47 (2006) 6387–6397
polymer
www.elsevier.com/locate/polymer

Crystallization of a miscible propylene/ethylene copolymer blend

Y.S. Hu [a,1], A.R. Kamdar [a], P. Ansems [b], S.P. Chum [b], A. Hiltner [a,*], E. Baer [a]

[a] *Department of Macromolecular Science and Engineering, Center for Applied Polymer Research, Case Western Reserve University, Cleveland, OH 44106, USA*

[b] *Polyolefins and Elastomers R&D, The Dow Chemical Company, Freeport, TX 77541, USA*

Received 22 May 2006; received in revised form 27 June 2006; accepted 28 June 2006
Available online 28 July 2006

Abstract

The crystallization behavior and morphological patterns of a miscible blend of two propylene/ethylene (P/E) copolymers that differed in ethylene content were studied. Metallocene-catalyzed P/E copolymers containing 3.1 and 11.0 mol% ethylene were chosen for blending. The difference in ethylene content was small enough to ensure miscibility of the pair in the melt, and the ethylene content was low enough to ensure that both were crystallizable. The blends were characterized by differential scanning calorimetry (DSC), wide angle X-ray diffraction (WAXD), optical microscopy (OM) and atomic force microscopy (AFM). The complex melting endotherm of the blends consisted of a broad low temperature peak at T_{m1}, a high temperature peak at T_{m2}, and an intermediate peak at T'_m which was not characteristic of either constituent and depended on blend composition. The multiple melting peaks arose from distinct crystal populations. All the blends exhibited a mixed morphological texture of α-radial lamellae with short, densely packed γ-overgrowths, interspersed with areas of α-crosshatch. The high temperature peak at T_{m2} was assigned to the melting of the α-radial lamellae which formed from chains of the lower comonomer constituent. The broad low temperature peak at T_{m1} was attributed to the melting of γ-crystal overgrowths on the radial lamellae. The new peak at T'_m was thought to arise from the melting of the α-crosshatch lamellae. The lamellar thickness, and hence T'_m, correlated with the crystallization temperature, which decreased as the blend was made richer in the higher comonomer constituent.

Keywords: Crystallization; Propylene copolymers; Miscible blends

1. Introduction

The miscibility and phase behavior of binary polymer blends is a subject of continuing academic and industrial interest. Fundamental studies of polymer miscibility often focus on blends of noncrystalline constituents. Nevertheless, blends that incorporate one or more crystallizable constituents are also of interest not only because crystalline polymers are of considerable commercial importance, but also because blending crystalline polymers offers an effective route to a wide range of morphological patterns and novel structure–property relationships.

If only one constituent of a miscible melt blend is crystallizable, crystallization is accompanied by segregation of the noncrystallizing constituent. The morphology is characterized by the distance over which the noncrystallizing constituent is expelled. Segregation can be at the interlamellar, interfibrillar, or interspherulitic levels [1].

Even more possibilities for complex morphologies exist if both constituents are crystallizable. In most cases, the lattice parameters do not match closely enough for the constituents to cocrystallize, and crystallization creates two crystal populations. The morphology is characterized by the lamellar arrangement of the two crystal species. The insertion mode, where the lamellae of both species combine in a single stack, has been observed for blends of polycarbonate and polycaprolactone [2–4]. The block mode, where the constituents form

* Corresponding author. Department of Macromolecular Science and Engineering, Case Western Reserve University, 10900 Euclid Ave., Cleveland, OH 44106-7202, USA.
E-mail address: ahiltner@case.edu (A. Hiltner).
[1] Present address: Polyolefins and Elastomers R&D, The Dow Chemical Company, Freeport, TX 77541, USA.

0032-3861/$ - see front matter © 2006 Elsevier Ltd. All rights reserved.
doi:10.1016/j.polymer.2006.06.063

separate lamellar stacks, has been observed in blends of poly(ethylene oxide) and poly(ethylene succinate) [1], in blends of poly(vinylidene fluoride) (PVDF) and poly(1,4-butylene adipate) [5], and in blends of PVDF and poly(3-hydroxybutyrate) [6].

When chain conformation and lattice parameters of the constituents match closely and the constituents exhibit similar crystallization kinetics, cocrystallization may occur. This is most often observed if the constituents are chemically similar. Examples include blends of ultrahigh molecular weight polyethylene (UHMWPE) with linear low density polyethylene (LLDPE) or with high density polyethylene (HDPE) [7], blends of LLDPE and HDPE [8,9], blends of polyethylene and its copolymers [10], and blends of isotactic polypropylene (iPP) with propylene/ethylene (P/E) random copolymers [11].

A recent study established that metallocene P/E (mP/E) copolymers are miscible in the melt if the difference in ethylene content is less than 18 mol% [12]. A natural extension is to examine the crystallization behavior and morphological patterns of a miscible mP/E blend. In the present study, mP/E copolymers containing 3.1 and 11.0 mol% ethylene are chosen for blending. The difference in ethylene content is small enough to ensure miscibility of the pair in the melt, and the ethylene content is low enough to ensure that both are crystallizable. Separately, both copolymers crystallize as a mixture of the polypropylene α-form and γ-form, although the total crystallinity is significantly higher in the copolymer with 3.1 mol% ethylene. The complex polymorphism and morphologies that are typical of P/E copolymers are examined with differential scanning calorimetry (DSC), wide angle X-ray diffraction (WAXD), optical microscopy (OM) and atomic force microscopy (AFM). The crystallization modes for miscible mP/E copolymer blends are extracted from the combined results.

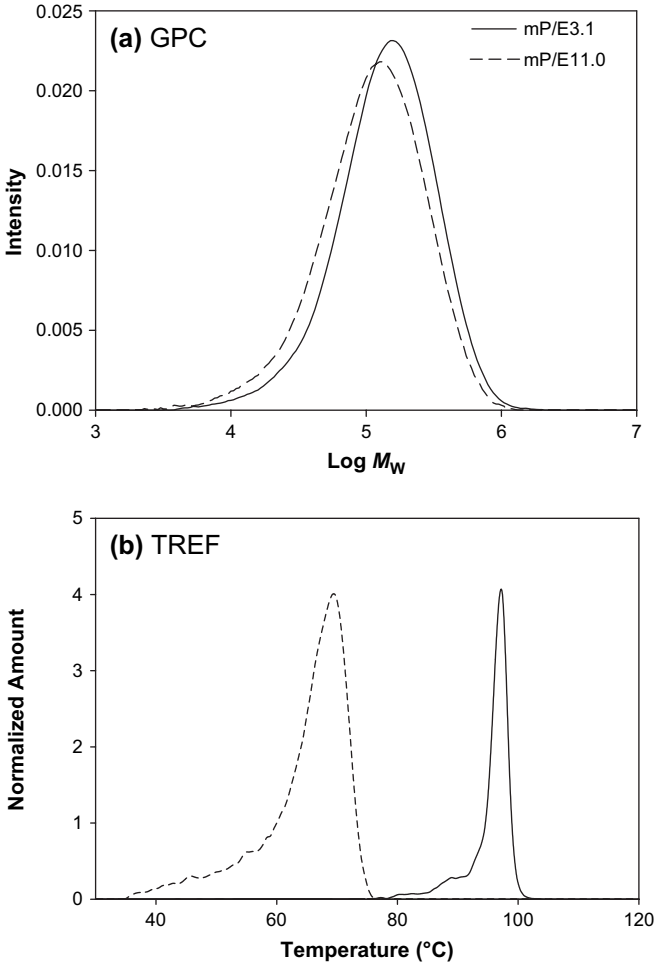

Fig. 1. (a) GPC and (b) TREF curves of mP/E3.1 and mP/E11.0.

2. Materials and methods

Two experimental metallocene-catalyzed P/E copolymers (mP/E) containing 3.1 and 11.0 mol% ethylene were supplied by The Dow Chemical Company (Freeport, TX) and are referred to as mP/E3.1 and mP/E11.0, respectively. The mP/E3.1 had weight average molecular weight $M_w = 341$ kg mol^{-1} and polydispersity = 2.2. The mP/E11.0 had $M_w = 147$ kg mol^{-1} and polydispersity = 2.1. The molecular weight distributions, provided by the manufacturer, were well approximated by a logarithmic normal distribution, Fig. 1a. The temperature rising elution fractionation (TREF) curves of the two copolymers were reasonably narrow, Fig. 1b. The mP/E3.1 eluted at a higher temperature in accordance with its higher crystallinity. The densities of compression molded plaques were measured at room temperature using a gradient column (ASTM D1505-85). The densities of mP/E3.1 and mP/E11.0 were 0.902 and 0.889 g cm^{-3}, respectively.

The two mP/Es were solution blended through the entire composition range. Typically the constituents were dissolved in 1,2,4-trichlorobenzene at 130 °C at a total concentration of 1% (w/w) and stirred at the same temperature for 2 h. The blend was precipitated from solution in chilled methanol with constant stirring. The mixture was centrifuged and the solvent was decanted. The resulting solid was vacuum dried at 60 °C for at least 48 h until constant weight was achieved. The dried blend was stabilized by spraying with 3000 ppm of Irganox1010/Irgafos168 in a 50/50 composition in acetone.

Thermograms were obtained with a Perkin Elmer DSC-7 from −60 to 190 °C. Specimens were heated to 190 °C for 5 min, cooled to −60 °C at various rates and subsequently heated at 10 °C min^{-1}. The crystallization enthalpy was determined from the cooling thermogram by extrapolation of the linear baseline in the melt region. It was characteristic that the cooling curves did not return to the baseline immediately following the sharp crystallization peak, which indicated that some amount of crystallization occurred below the peak temperature. The temperature range of the enthalpic contribution extended below the onset melting temperature in the subsequent heating thermogram, although this was not always apparent in the figures because of the scale difference between the cooling and melting thermograms.

The temperature modulated DSC scans were obtained with a TA Instruments 2920 DSC. A heating ramp of 3 °C min^{-1} was used after specimens were cooled at 10 °C min^{-1} to 20 °C.

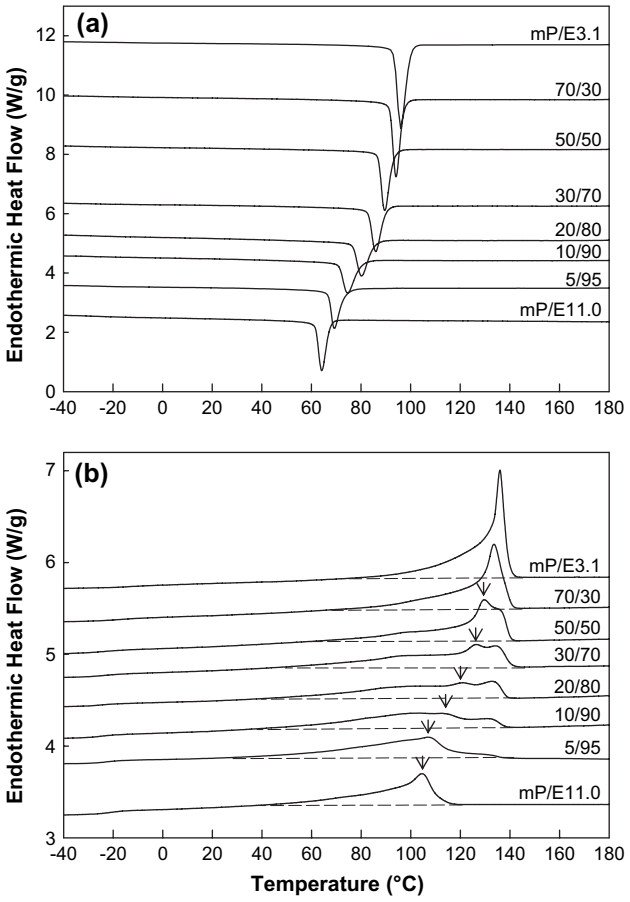

Fig. 2. Thermograms of mP/E3.1, mP/E11.0 and their blends obtained with a cooling/heating rate of 10 °C min^{-1}. (a) Cooling curves and (b) subsequent heating curves. The curves are shifted for clarity.

Wide angle X-ray diffraction (WAXD) was performed at room temperature in a Rigaku DMAX 2000/PC diffractometer with Cu$K_{\alpha 1}$ radiation and at a scanning increment of 0.05°. The determination of the γ-crystal fraction followed the protocol developed by Turner-Jones [13].

Free surfaces for atomic force microscopy (AFM) were prepared by melting the polymer on a glass slide at 190 °C and cooling at a controlled rate. Specimens were imaged immediately. To expose the interior morphology, the 30/70 blend was microtomed at −75 °C and etched at ambient temperature for 10 min using a solution containing 0.7 w/v% of potassium permanganate dissolved in a 1:4 v/v sulfuric acid:*o*-phosphoric acid solution. The AFM experiments were conducted in air at ambient conditions using the Nanoscope IIIa MultiMode head from Digital Instruments (Santa Barbara, CA) in the tapping mode. The tip radius was 10 nm. Phase and height images were recorded simultaneously.

3. Results and discussion

3.1. Crystallization and melting thermograms

The thermograms of mP/E3.1, mP/E11.0 and their blends were obtained by cooling from 190 to −60 °C at a rate of 10 °C min^{-1}, Fig. 2a, followed by heating at the same rate, Fig. 2b. The cooling curve of mP/E3.1 revealed a sharp crystallization peak at a temperature T_c of 96 °C with a crystallization enthalpy ΔH_c of 86 J g^{-1}. The heating curve showed a sharp melting peak at a temperature T_m of 136 °C. The heat of melting ΔH_m corresponded to the heat of crystallization. Due to the higher ethylene content, mP/E11.0 exhibited a lower T_c of 64 °C and a smaller ΔH_c of 53 J g^{-1}. The subsequent heating curve showed a broad melting peak with the peak temperature at 105 °C.

A single sharp crystallization peak was observed for all the blend compositions, which is consistent with crystallization from a miscible melt [9,14]. The crystallization temperatures and transition enthalpies of the blends were intermediate between those of mP/E3.1 and mP/E11.0. The linear relationship between crystallization enthalpy or melting enthalpy and blend composition, Fig. 3a, indicated additive contributions of mP/E3.1 and mP/E11.0 to the total crystallinity. In contrast, the crystallization temperature showed pronounced nonlinear behavior. The crystallization temperature was only slightly reduced from that of mP/E3.1 if mP/E3.1 was the major constituent of the blend, Fig. 3b. This suggested that the higher crystallinity constituent had a strong nucleating effect on crystallization of the miscible blend.

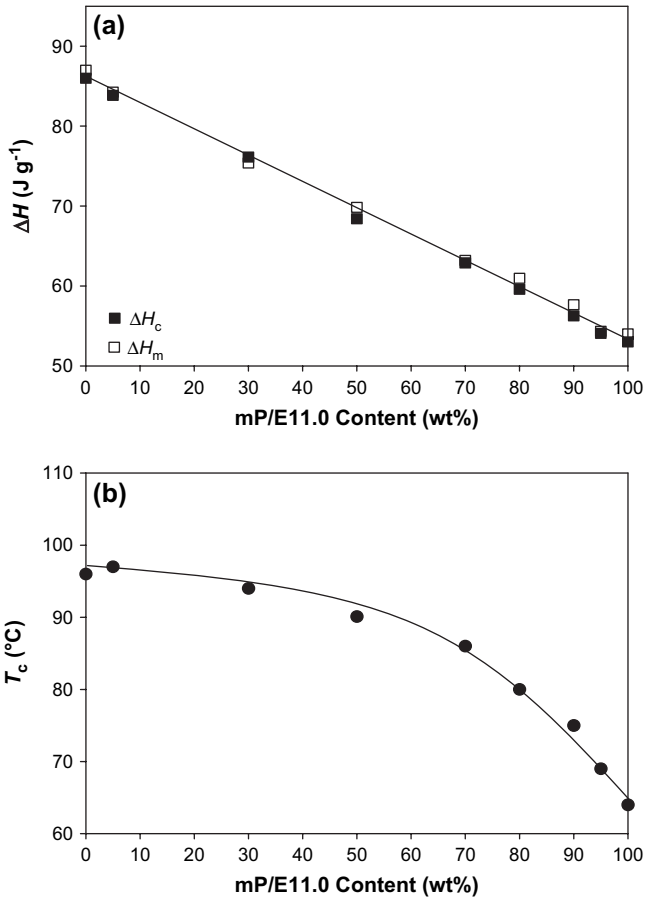

Fig. 3. (a) Melting and crystallization enthalpies as a function of mP/E11.0 content and (b) crystallization temperature T_c as a function of mP/E11.0 content.

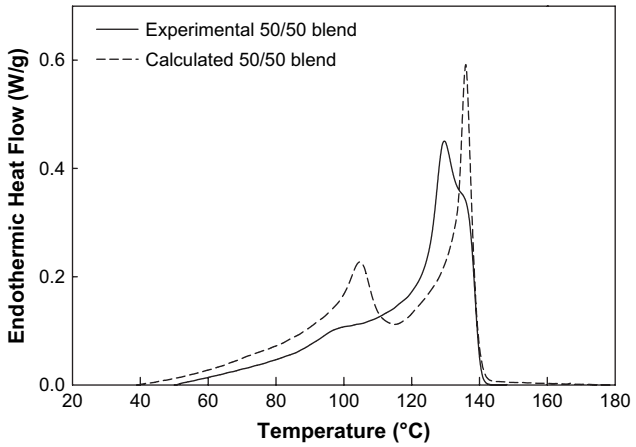

Fig. 4. Comparison of the melting behavior of a 50/50 blend with that calculated from the additive contributions of mP/E3.1 and mP/E11.0.

The complex melting endotherm of the blends consisted of a broad low temperature peak at T_{m1}, an intermediate peak at T'_m (indicated by an arrow) and a high temperature peak at T_{m2}, Fig. 2b. Although the blend constituents contributed additively to the total melting enthalpy, the shape of the melting endotherm was not an additive combination of the constituent endotherms. This is clearly shown in Fig. 4, which compares the heating thermogram of a 50/50 blend with the additive thermogram calculated from the thermograms of mP/E3.1 and mP/E11.0. The experimental curve had significantly weaker intensity than the calculated one at the melting temperatures corresponding to mP/E3.1 and mP/E11.0. Because ΔH_m obeyed the rule of mixtures, it could be concluded that both constituents contributed to the new peak at T'_m. Possibly, fractions from both constituents cocrystallized as a distinct morphology. Of the three melting peaks, T'_m was the one most strongly dependent on T_c. Indeed, as the concentration of mP/E11.0 increased, T'_m decreased linearly with T_c according to $T'_m = T_c + 40\,^{\circ}C$, Fig. 5. The linear relationship suggested that the thickness of crystals associated with T'_m decreased with increasing concentration of mP/E11.0.

The appearance of multiple melting peaks can usually be explained by the coexistence of different crystal populations

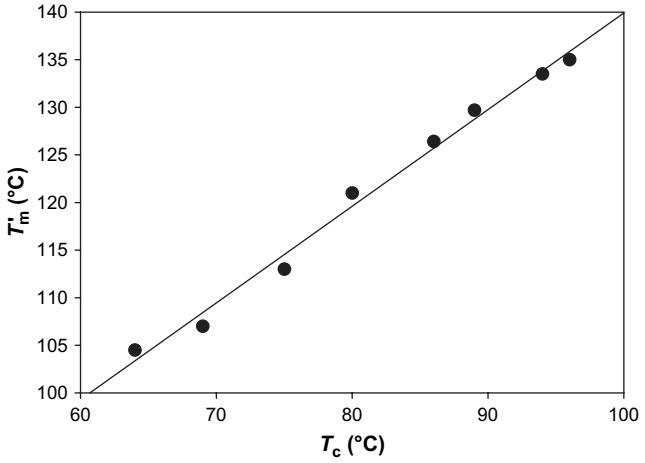

Fig. 5. T'_m as a function of crystallization temperature T_c.

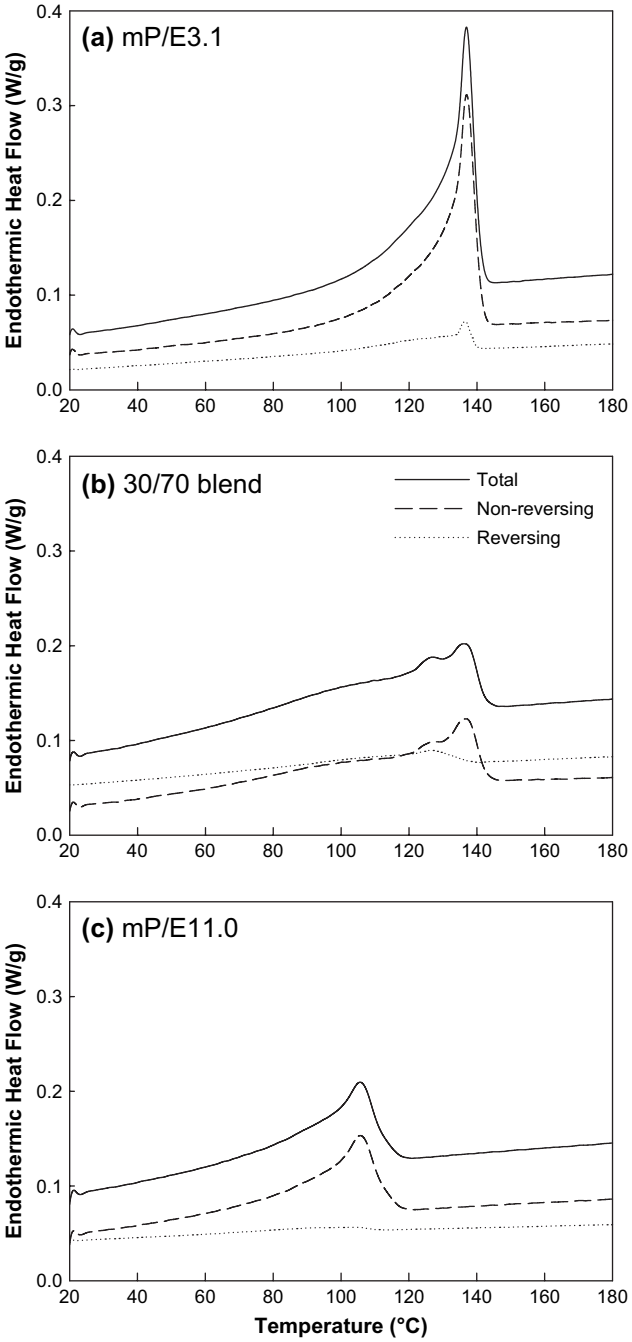

Fig. 6. Temperature modulated DSC heating thermograms at 3 °C min^{-1} after cooling at 10 °C min^{-1}. (a) mP/E3.1, (b) 30/70 blend, and (c) mP/E11.0.

or alternatively by melting and recrystallization. The possibilities were differentiated by temperature modulated DSC using a 3 °C min^{-1} heating ramp after 10 °C min^{-1} cooling, Fig. 6. This technique provides the total heat flow as from a conventional DSC and the reversible component of the heat flow. The difference between the reversing signal and the total signal is the non-reversing component. In the case of semicrystalline polymers, the non-reversing endothermic signal is typically due to complete melting of lamellae, whereas the reversing endothermic signal is due to partial melting of lamellae and subsequent rapid recrystallization [15]. For mP/E3.1, the

reversing signal made a very small contribution to the melting peak at 138 °C. For both mP/E3.1 and mP/E11.0, the non-reversing component represented essentially the total curve; the reversing component made little or no contribution. A small peak in the reversing curve of the 30/70 blend at 128 °C indicated that some amount of partial melting and reorganization was associated with T'_m. Nevertheless, the non-reversing component represented most of the curve including the peak at T'_m. Consequently, it was concluded that the multiple peaks in the melting endotherms of mP/E3.1/mP/E11.0 blends were primarily due to the coexistence of different crystal populations and not due to melting and recrystallization.

3.2. Crystal structure

Wide angle X-ray diffraction patterns of films cooled at 10 °C min^{-1} from 190 to 20 °C are shown in Fig. 7a. The characteristic peaks of the polypropylene α-form appear at 2θ of 14.1° (110), 16.7° (040), 18.6° (130), 21.1° (111) and 21.9° (041). The X-ray diffraction pattern of the polypropylene γ-form is similar to that of the α-form in many respects, however, the strong reflection of the α-form at 18.6° is absent in the γ-form and a reflection appears at 20.1° (040). The ratio of the α-form (130) peak intensity to the γ-form (040) peak intensity was used to calculate the relative contribution of each form to the total crystallinity [13]. The mP/E3.1 and mP/E11.0 showed 30% and 72% γ-form, respectively. These values were reasonable in view of a literature report that described a propylene copolymer with 4.4 mol% ethylene as having about 50% γ-form when crystallized in the temperature range of 116–136 °C [16]. The presence of short isotactic propylene sequences due to disruption by comonomer units promoted formation of the γ-form [17–20]. The γ-form concentration in the blends was intermediate between those of mP/E3.1 and mP/E11.0 and increased almost linearly with increasing amount of mP/E11.0, Fig. 7b.

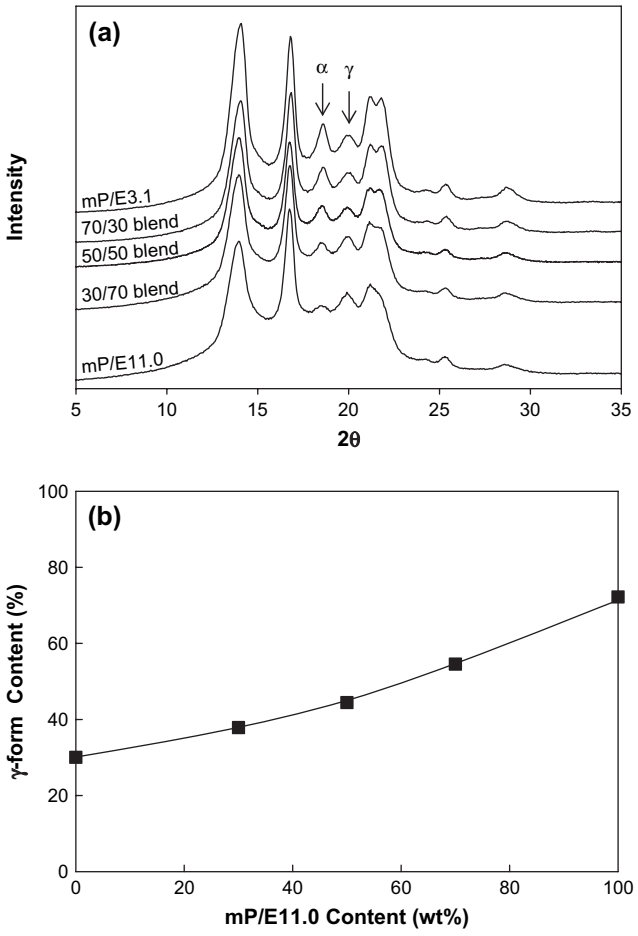

Fig. 7. Determination of the γ-form content. (a) WAXD scans and (b) amount of γ-form as a function of mP/E11.0 content.

3.3. Crystalline morphology

When cooled at 10 °C min^{-1}, mP/E3.1, mP/E11.0 and the blends crystallized as space-filling spherulites. Spherulites of mP/E3.1 had a diameter of 20–30 μm and positive or mixed birefringence. The positive sign indicated that the chain direction was radial in a significant fraction of the lamellae. Because the chains were perpendicular to the lamellar surface, these lamellae were oriented in the tangential direction with respect to the spherulite growth direction. With increasing mP/E11.0 content, the spherulites of the blends became smaller and more irregular. When viewed under crossed polarizers, the sign of the birefringence remained positive or mixed for all the blends. The mP/E11.0 produced very small irregular spherulites about 5 μm in diameter with mostly negative birefringence, indicating a tendency for radial lamellar orientation. Secondary crystallization by crystallographic branching from radial lamellae occurs infrequently or slowly in propylene copolymers [21].

The high resolution AFM phase images of free surfaces in Fig. 8 reveal the lamellar structure of specimens cooled at 10 °C min^{-1}. The long, radial lamellae in mP/E3.1 indicated as A are often referred to as laths or radial lamellae with α-form crystals, Fig. 8a. They are oriented edge-on with thickness in the range of 16–22 nm. The edge-on tangential lamellae indicated as B are thinner, in the range of 13–16 nm. They are referred as "α-overgrowths" because the angle of 80° between these tangential lamellae and the α-lath suggests that they are α-branches formed by epitaxial growth on the (010) plane of the radial α-lath.

In some regions indicated by C, the parent lamellae and their branches form a densely packed α-crosshatch. This often occurs in the interspherulitic regions but also between radial arms of the spherulite where the α-crosshatch has space to grow and develop. These lamellae have a thickness in the same range as the α-overgrowths.

In other regions, densely packed small edge-on crystals indicated as D grow from the α-laths. Often these crystals are so densely packed that the underlying α-lath is not visible. These lamellae, 12–14 nm in thickness, are thinner than α-overgrowth lamellae. Their identification as γ-overgrowths is consistent with assignments by Thomann [18] and Alamo [22,23]. An identical γ-overgrowth texture is reported in isotactic polypropylene [24]. The γ-overgrowths nucleate from the (010) edges of the α-lamellae at a 40° angle to the fold plane, which results in parallel alignment of the chain axes of the two

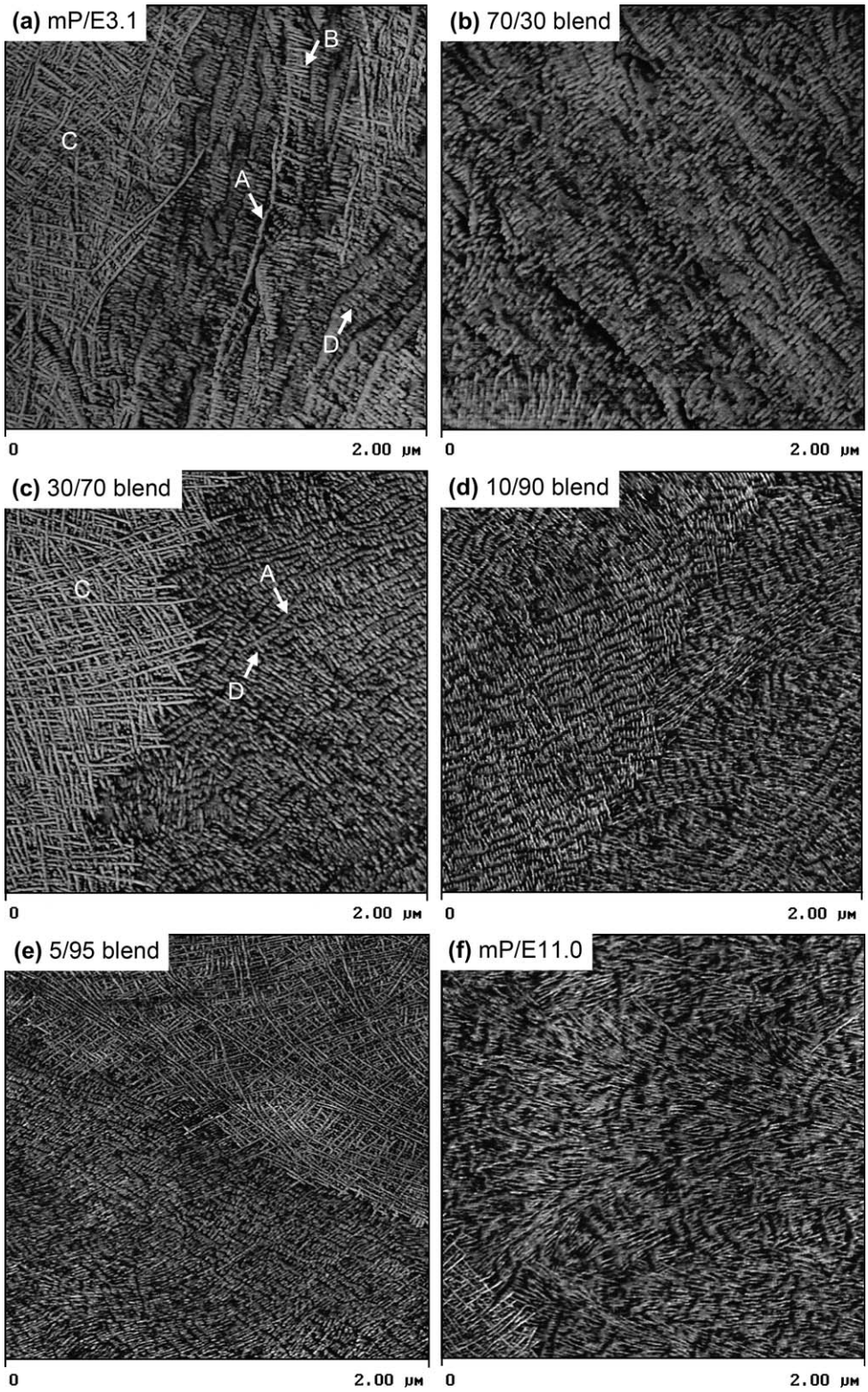

Fig. 8. AFM phase images of free surfaces cooled at 10 °C min^{-1}. (a) mP/E3.1, (b) 70/30 blend, (c) 30/70 blend, (d) 10/90 blend, (e) 5/95 blend, and (f) mP/E11.0.

crystal forms [25,26]. When the γ-lamellae are viewed edge-on, the underlying α-lath is tilted by 40° out of the plane. Consequently, the α-lath is obscured by the closely packed stacks of γ-lamellae. A large population of tangential α- and γ-overgrowths is consistent with the positive birefringence observed under the optical microscope.

The 70/30 blend also crystallized as α-laths with numerous short overgrowths interspersed with areas of α-crosshatch, Fig. 8b. However, the α-overgrowths with their characteristic 80° angle were not readily apparent; rather, stacks of γ-overgrowth crystals on the underlying α-laths predominated. An increase in the fraction of γ-crystals was consistent with the

Table 1
Thermal properties and morphological features of mP/E3.1/mP/E11.0 blends

Blend composition	γ-Form content (%)	DSC cooling (10 °C min^{-1})		Reheating (10 °C min^{-1})	Spherulite size (μm)	α-Crosshatch lamellae (nm)	γ-Form lamellae (nm)
		T_c (°C)	ΔH_c (J g^{-1})	ΔH_m (J g^{-1})			
mP/E3.1	30	96	86	87	20–30	13–16	10–14
70/30	38	94	76	75	10–25	13–16	10–14
30/70	55	86	63	63	5–20	12–14	10–12
10/90	–	75	56	58	5–10	8–11	7–8
5/95	–	69	54	54	5–10	8–10	6–8
mP/E11.0	72	64	53	54	5	7–10	7–9

increase in percentage of γ-form from 30% for mP/E3.1 to 38% for the 70/30 blend as determined by WAXD. However, the thickness of the crosshatch lamellae and the γ-crystals remained the same as in mP/E3.1.

All the blends exhibited a mixed morphological texture of α-radial lamellae (A) with short, densely packed γ-overgrowths (D), interspersed with areas of α-crosshatch (C), Fig. 8c–e. As the concentration of mP/E11.0 increased, α-radial lamellae became shorter and the densely packed γ-overgrowth lamellae became shorter and thinner. The α-crosshatch lamellae also became thinner. The lamellar thicknesses are compiled in Table 1. The trend with increasing mP/E11.0 toward shorter α-radial lamellae with densely packed γ-overgrowth crystals was consistent with increasing fraction of γ-crystals.

The morphology of mP/E11.0 was dominated by short lamellae with a tendency toward radial organization, Fig. 8f. This confirmed the interpretation of the negative optical birefringence. These lamellae, with thickness in the range of

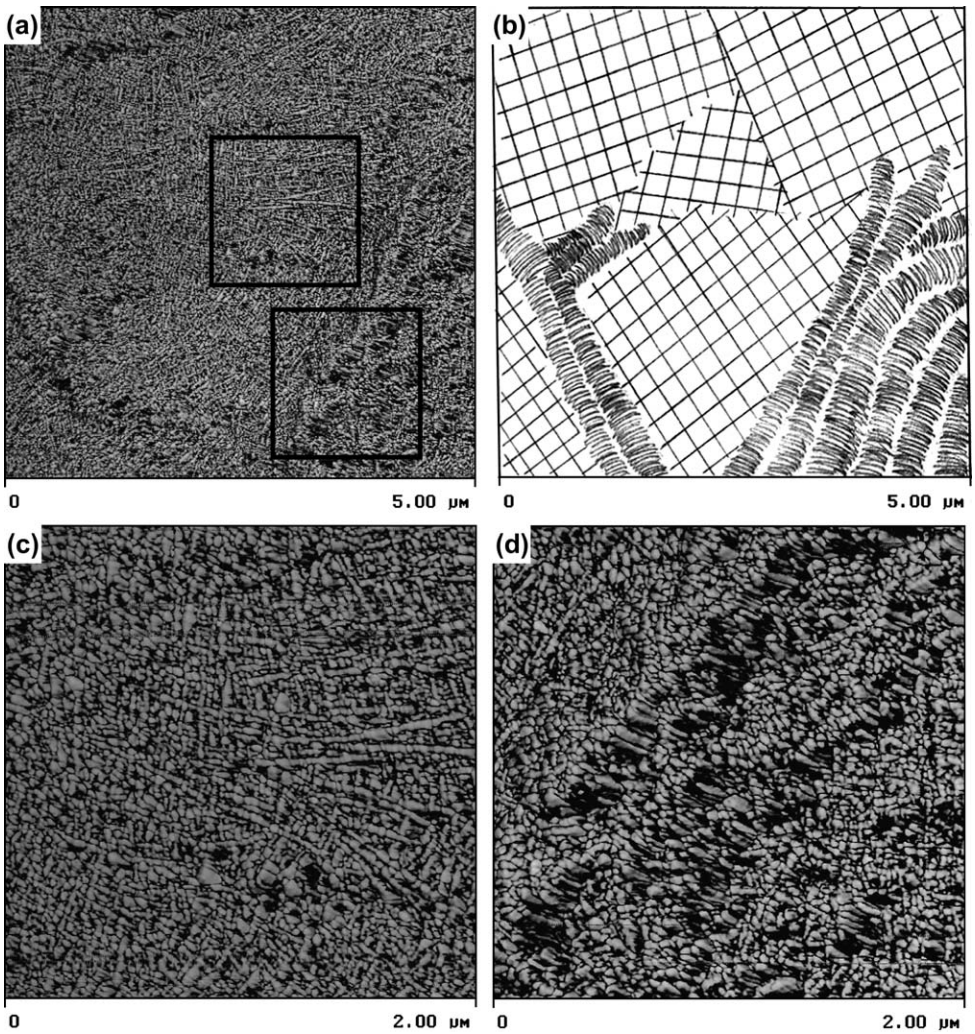

Fig. 9. AFM phase images of the 30/70 blend after it was microtomed and etched. (a) Lower resolution image showing α-crosshatched lamellae filling the space between radial arms of a spherulite, (b) schematic drawing of the morphology in (a), (c) higher resolution image of the α-crosshatched region, and (d) higher resolution image of the spherulite arms showing the short γ-overgrowth lamellae.

7–10 nm, frequently appeared as stacks or bundles. They were probably γ-crystals, as mP/E11.0 had 72% γ-form. A similar lamellar organization was found in a P/E copolymer containing 8.2 mol% defects and almost 100% γ-crystals [22]. Occasionally, areas between the small spherulites contained α-crosshatch lamellae, which accounted for the 28% α-form as determined by WAXD. However, there was no indication of the α-laths or α-radial lamellae with the characteristic stacks of γ-overgrowths that were typical of blends with as little as 5 wt% mP/E3.1.

It was possible that some of the morphological features in Fig. 8 resulted from crystallization at a free surface. To determine whether the surface features reflected the bulk morphology, a 30/70 blend was microtomed and the interior surface was lightly etched to reveal the crystalline texture. The lower resolution image in Fig. 9a shows a large region of α-crosshatched lamellae filling the space between radial arms of a spherulite. For clarity, the morphological features are sketched in Fig. 9b. A higher resolution image confirms the crosshatched texture, Fig. 9c. The granular appearance of the fragile lamellae might have been a result of the etching process. A higher resolution image of a spherulite arm shows the short, densely packed γ-overgrowth crystals that obscure the underlying α-laths, Fig. 9d. These images confirmed that the morphological features observed on free surfaces were representative of the interior morphology of the blends.

3.4. Effect of cooling rate

Decreasing the cooling rate resulted in a systematic increase in the fraction of γ-crystals of mP/E3.1, mP/E11.0 and their blends, Fig. 10. For example, the γ-form in the 30/70 blend increased from 39% to 55% to 69% as cooling rate decreased from 30 to 10 to 3 °C min^{-1}. A lower cooling rate increased the crystallization temperature and prolonged the crystallization time, which favored formation of the γ-crystal form, as has been shown with isotactic polypropylene containing structural defects or comonomer units [17,19].

The crystallization thermograms of the mP/E3.1/mP/E11.0 30/70 blend obtained at several cooling rates, and the subsequent melting thermograms obtained at 10 °C min^{-1} are shown in Fig. 11a,b. The single sharp crystallization peak shifted to higher temperature as the cooling rate decreased. In the subsequent heating thermogram, the total melting enthalpy was not affected by the cooling rate. However, as the cooling rate decreased, the broad low temperature melting

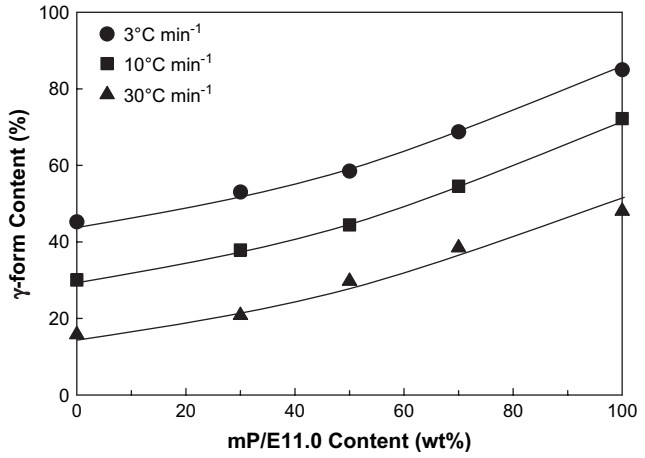

Fig. 10. Effect of cooling rate on the amount of γ-form determined by WAXD.

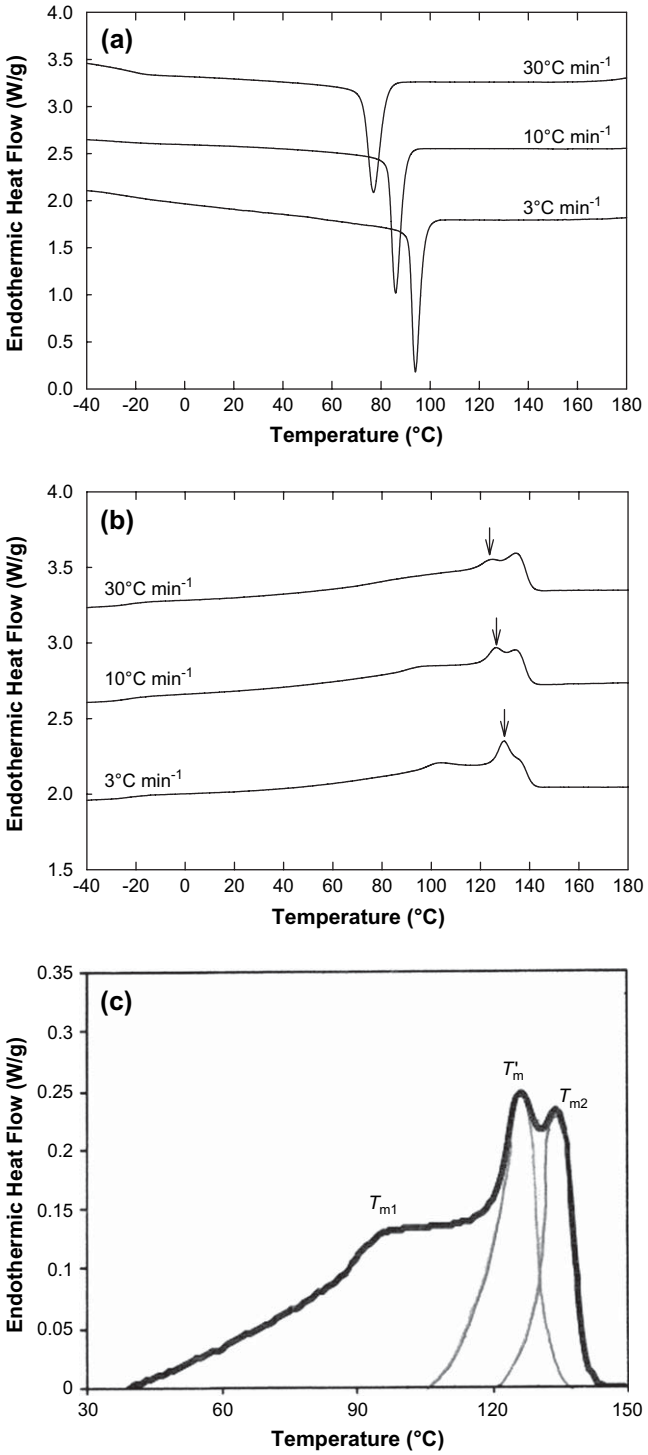

Fig. 11. Effect of cooling rate on crystallization and melting behaviors of the 30/70 blend. (a) Cooling thermograms obtained with the cooling rates indicated, (b) subsequent heating thermograms obtained with a heating rate of 10 °C min^{-1}, and (c) deconvolution of the melting endotherm. The curves are shifted for clarity.

Table 2
Effect of cooling rate on thermal behavior and morphological features of mP/E3.1/mP/E11.0 30/70 blends

Cooling rate (°C min^{-1})	γ-Form content (%)	DSC cooling		DSC heating at 10 °C min^{-1}				γ-Overgrowth lamellar thickness (nm)	γ-Overgrowth lamellar length (nm)	α-Crosshatch lamellar thickness (nm)
		T_c (°C)	ΔH_c (J g^{-1})	ΔH_m (J g^{-1})	f_1	f'	f_2			
30	39	77	62	62	0.47	0.28	0.26	7–11	40–90	10–14
10	55	86	63	63	0.54	0.27	0.19	10–12	40–130	12–14
3	69	94	64	64	0.61	0.32	0.07	10–15	160–250	12–20

peak at T_{m1} and the intermediate peak at T'_m (arrows) became more pronounced, whereas the intensity of the high temperature peak at T_{m2} was reduced. In addition, T'_m increased from 124 to 130 °C as the cooling rate decreased from 30 to 3 °C min^{-1}, which was consistent with the relationship between T'_m and T_c (see Fig. 5). All the transition temperatures and enthalpies are listed in Table 2.

The contribution of each peak to the total enthalpy was obtained by deconvoluting the thermogram as shown in Fig. 11c. The peaks at T'_m and T_{m2} were approximated with two Gaussian distributions and the corresponding contributions to the enthalpy f' and f_2, were defined as the ratio of the peak area to the total area. The contribution from T_{m1}, given as $f_1 = 1-(f'+f_2)$, was about 0.47 for a cooling rate of 30 °C min^{-1}, and increased to 0.61 for a lower rate of 3 °C min^{-1}. For the different cooling rates, f_1 corresponded roughly to the concentration of γ-crystals as determined by WAXD, Table 2.

Regardless of the cooling rate, the morphology of mP/E3.1/mP/E11.0 30/70 blend exhibited a mixture of α-radial lamellae with short, densely packed γ-overgrowths, interspersed with areas of α-crosshatch. It was not possible to determine from the AFM images whether cooling rate affected the relative amount of the two textures. However, the α-crosshatch lamellae became thicker as the cooling rate decreased, which was consistent with the increase in T_c and T'_m. The γ-overgrowths on underlying α-radial lamellae are shown in Fig. 12. As the cooling rate decreased from 30 to 3 °C min^{-1}, the γ-overgrowths increased in thickness from 7–11 nm to 10–15 nm, and the length increased from 40–90 nm to 160–250 nm, Table 2. The thickening and lengthening of γ-overgrowths with decreasing cooling rate was consistent with the increase in γ-form content from WAXD.

3.5. Crystallization model

The crystallization habits of miscible mP/E3.1/mP/E11.0 blends under the conditions used in this study can now be discussed in terms of the DSC, WAXD and AFM results. The multiple melting peaks in the DSC thermogram arise from distinct crystal populations, rather than from melting and recrystallization, as is shown by temperature modulated DSC. The high temperature peak at T_{m2} is assigned to the melting of the α-laths and α-radial lamellae. These entities crystallize first upon cooling from the melt. They are comprised of fractions with the longest isotactic propylene sequences and lowest comonomer defects. The α-laths and α-radial lamellae constitute the underlying skeleton of the irregular spherulites and they provide a substrate for epitaxial crystallization of the γ-overgrowths and the rare α-overgrowths. Chains that form the α-laths are provided by the mP/E3.1 constituent. As the concentration of mP/E11.0 increases, the α-laths become shorter due to the dilution of mP/E3.1. However, 5 wt% of mP/E3.1 provides enough chains to form α-radial lamellae.

The broad low temperature peak at T_{m1} is attributed to the melting of γ-crystal overgrowths. This assignment is supported by the correlation between the enthalpic contribution of this peak and the γ-form content measured by WAXD (see Table 2). These crystals also form the thinnest lamellae, which are consistent with the low melting temperature. The low melting temperature of γ-crystals has also been noticed in propylene homopolymer and in propylene/ethylene copolymers [13,20]. Chains from both blend constituents are thought to contribute to γ-overgrowth crystallization; however, a larger fraction of the crystallizable mP/E11.0 chains crystallize in the γ-form. The presence of short isotactic propylene sequences due to frequent disruption by comonomer units in mP/E11.0 favors formation of the γ-form. It appears that mP/E11.0 does not contain a fraction with isotactic sequences long enough to form the α-radial lamellae. In the absence of mP/E3.1, the γ-crystals of mP/E11.0 form short, more-or-less radially oriented lamellae.

The new endothermic peak at T'_m is attributed to the melting of α-crosshatch lamellae. This assignment is based on the observed correlation between α-crosshatch lamellar thickness and T'_m. A previous study of propylene homopolymers crystallized under special conditions also suggests that α-crosshatch lamellae melt at a lower temperature than the α-radial lamellae [27]. The α-crosshatch incorporates chain fractions from both constituents. This is inferred from the non-additivity of the thermograms (see Fig. 4). Existence of fractions in both constituents that can crystallize as α-crosshatch is confirmed by the observation of α-crosshatch in both mP/E3.1 and mP/E11.0 when they are crystallized separately. The α-crosshatch appears to grow independently of the α-radial lamellae, mostly in interspherulitic pockets and in the regions between the radial lamellar arms.

4. Conclusions

Copolymers of propylene and ethylene are miscible over a fairly wide range in copolymer composition. Regardless of comonomer content, the propylene-rich copolymers all take the same crystal form. Copolymer composition only affects the total crystallinity and the relative amounts of the polypropylene

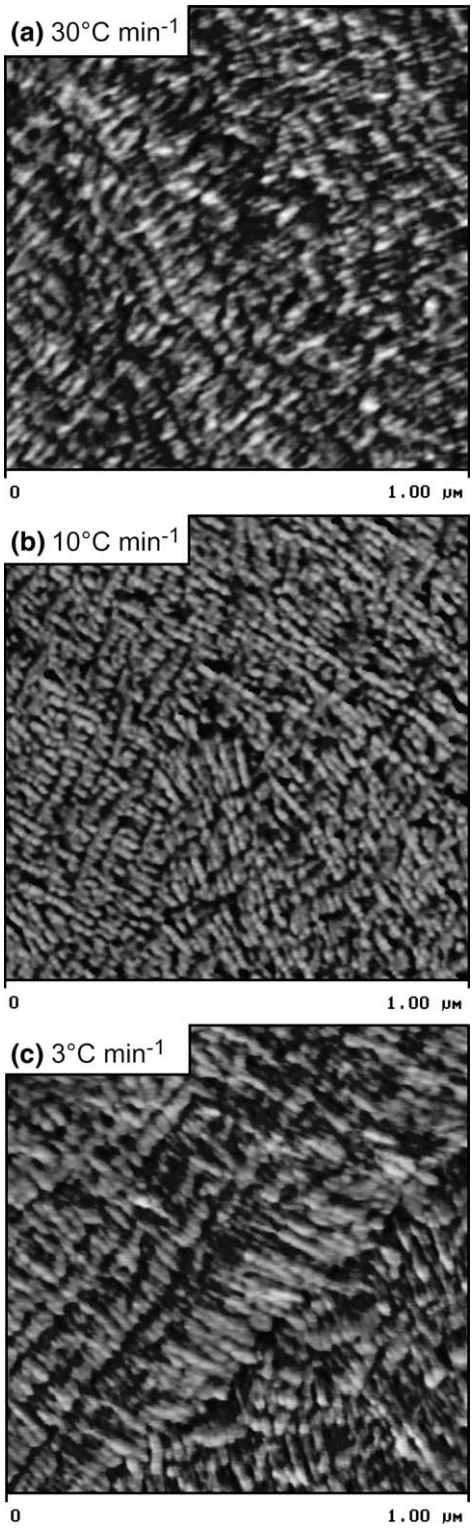

Fig. 12. AFM phase images of 30/70 blend free surface cooled at different rates. (a) 30 °C min^{-1}, (b) 10 °C min^{-1}, and (c) 3 °C min^{-1}.

α- and γ-forms. These factors favor cocrystallization of the blend constituents. On the other hand, comonomer content strongly affects the crystallization kinetics, which favors separate crystallization of the constituents. Both features are found in this study of the crystallization behavior and morphological patterns of a miscible blend of metallocene-catalyzed propylene/ethylene copolymers containing 3.1 and 11.0 mol% ethylene.

The complex melting endotherm of the blends consisted of a broad low temperature peak at T_{m1}, a high temperature peak at T_{m2}, and an intermediate peak at T'_m which was not characteristic of either constituent and depended on the crystallization temperature. The multiple melting peaks were identified with distinct crystal populations. The high temperature peak at T_{m2} was associated with melting of α-radial lamellae that formed from chains of the lower comonomer constituent. These chains had the longest isotactic sequences and the fewest comonomer defects. These lamellae formed the radial arms of the space-filling spherulites. The α-radial lamellae provided a substrate for epitaxial crystallization of both constituents as γ-overgrowths and rarely as α-overgrowths. The tangential lamellae were numerous enough to impart positive birefringence to the spherulites. The broad low temperature peak at T_{m1} was attributed to the melting of γ-overgrowths. Interspersed were areas of α-crosshatch lamellae. The new melting peak at T'_m was attributed to the α-crosshatch lamellae. The lamellar thickness and T'_m correlated with the crystallization temperature, which decreased as the blend was made richer in the higher comonomer constituent. Chains of both constituents contributed to the α-crosshatch.

Acknowledgments

The temperature modulated DSC measurements were generously provided by Drs. Galeski and Piorkowska of the Center of Molecular and Macromolecular Studies, Lodz, Poland. The authors thank The Dow Chemical Company for financial and technical support.

References

[1] Chen H-L, Wang S-F. Polymer 2000;41:5157–64.
[2] Cheung YW, Stein RS, Wignall GD, Yang HE. Macromolecules 1993; 26:5365–71.
[3] Cheung YW, Stein RS, Jin JS, Wignall GD. Macromolecules 1994; 27:2520–8.
[4] Cheung YW, Stein RS, Chu B, Wu G. Macromolecules 1994;27: 3589–95.
[5] Penning JP, Manley RSJ. Macromolecules 1996;29:84–90.
[6] Chiu H-J, Chen H-L, Lin JS. Polymer 2001;42:5749–54.
[7] Kyu T, Vadhar P. J Appl Polym Sci 1986;32:5575–84.
[8] Tashiro K, Satkowski MM, Stein RS, Li Y, Chu B, Hsu SL. Macromolecules 1992;25:1809–15.
[9] Schuman T, Stepanov EV, Nazarenko S, Capaccio G, Hiltner A, Baer E. Macromolecules 1998;31:4551–61.
[10] Alamo RG, Glaser RH, Mandelkern L. J Polym Sci Part B Polym Phys 1988;26:2169–95.
[11] Kim M-H, Alamo RG, Lin JS. Polym Eng Sci 1999;39:2117–31.
[12] Kamdar AR, Hu YS, Ansems P, Chum SP, Hiltner A, Baer E. Macromolecules 2006;39:1496–506.
[13] Turner-Jones A. Polymer 1971;12:487–508.
[14] Bensason S, Nazarenko S, Chum S, Hiltner A, Baer E. Polymer 1997;38:3513–20.
[15] Sauer BB, Kampert WG, Blanchard EN, Threefoot SA, Hsiao BS. Polymer 2000;41:1099–108.

[16] Mezghani K, Phillips PJ. Polymer 1995;36:2407–11.
[17] Alamo RG, Kim M-H, Galante MJ, Isasi JR, Mandelkern L. Macromolecules 1999;32:4050–64.
[18] Thomann R, Semke H, Maier R-D, Thomann Y, Scherble J, Mülhaupt R, et al. Polymer 2001;42:4597–603.
[19] Hosier IL, Alamo RG, Esteso P, Isasi JR, Mandelkern L. Macromolecules 2003;36:5623–36.
[20] Marigo A, Causin V, Marega C, Ferrari P. Polym Int 2004;53:2001–8.
[21] Poon B, Rogunova M, Chum SP, Hiltner A, Baer E. J Polym Sci Part B Polym Phys 2004;42:4357–70.
[22] Hosier IL, Alamo RG, Lin JS. Polymer 2004;45:3441–55.
[23] Alamo RG, Ghosal A, Chatterjee J, Thompson KL. Polymer 2005;46:8774–89.
[24] Zhou J-J, Liu J-G, Yan S-K, Dong J-Y, Li L, Chan C-M, et al. Polymer 2005;46:4077–87.
[25] Lotz B, Graff S, Wittmann JC. J Polym Sci Part B Polym Phys 1986;24:2017–32.
[26] Lotz B, Wittmann JC. J Polym Sci Part B Polym Phys 1986;24:1541–58.
[27] Weng J, Olley RH, Bassett DC, Jääskeläinen P. J Macromol Sci Part B Phys 2002;B41:891–908.